



Research Article

Investigation on the Ground Pressure Induced by Hard Roof Fracturing at Different Layers during Extra Thick Coal Seam Mining

Rui Gao ^{1,2}, Jingxuan Yang ³, Tiejun Kuang^{3,2} and Hongjie Liu²

¹College of Mining Engineering, Taiyuan University of Technology, Shanxi 030024, China

²Datong Coal Mine Group Co. Ltd., Datong 037000, China

³State Key Laboratory of Coal Resources and Safe Mining, China University of Mining & Technology, Xuzhou 221116, China

Correspondence should be addressed to Rui Gao; cumtgaorui@163.com and Jingxuan Yang; jxyangcumt@126.com

Received 1 June 2020; Revised 25 July 2020; Accepted 25 September 2020; Published 5 November 2020

Academic Editor: Yingchun Li

Copyright © 2020 Rui Gao et al. This is an open access article distributed under the Creative Commons Attribution License, which permits unrestricted use, distribution, and reproduction in any medium, provided the original work is properly cited.

The fracturing of hard roofs in different layers would result in complex ground pressure on the working face, such as supports collapsed and severe roadway deformation. However, the mechanism of the ground pressure induced by hard roof fracturing in different layers is still unclear. In the paper, a physical model of a 20 m extrathick coal seam mined with hard roofs existing was established based on the physical simulation similarity criterion. The overburden fracturing structure, abutment stress distribution, and failure characteristics of the coal body were monitored by a noncontact strain measurement system and resistance strain gauges, to reveal the mechanism of ground pressure induced by hard roof fracturing. Furthermore, *on-site* measurement was used to monitor and analyze the ground pressure affected by hard roofs in different levels. The results provide a theoretical basis for the control of ground pressure in extrathick coal seam mining with hard roofs.

1. Introduction

In coal seam mining, when hard roofs exist in the overburden, the breaking span is usually huge due to their great strength, thus would result in a strong ground pressure in the mining panel such as support failure and roadway deformation. Through numerical simulation and field measurement, He et al. and Wang et al. found that the large suspended area of hard roofs would easily cause a stress concentration and failure in advanced coal rock mass [1, 2]. When hard roof fracturing, the intensity of the energy release is higher due to the large breaking span. Ning et al. [3] studied the fracture energy of thick hard roofs by means of microseismic monitoring. The results showed that the high energy released by the breaking of thick and hard roofs is the main reason causing strong ground pressure. Bednarek and Majcherczyk [4] discussed the rock mass characteristics which influence the choice of support. Zhao et al. [5] studied the fracture characteristic of an extrathick and hard roof based on the long beam theory. Li et al. [6] studied the periodic

breaking span of a thick and hard roof based on the Vlasov plate theory and the strain energy distribution characteristics of coal seam under a thick hard roof. Shen et al. [7] revealed the strong response for an entry influenced by overlying hard roof and the influence of the hard roof fracture position on the entry. Ju and Xu [8] analyzed the structural characteristics of overlying hard strata and ground pressure in the panel after a 7 m-thick coal seam mining. Xia et al. [9] studied the characteristics and mechanism of ground pressure in the mining panel under the combined action of hard roofs and a coal pillar. It was found in the above research that, because of the high strength and large overhang of hard roofs, the stress concentration is obviously on the hard roofs, which has a significant impact on the working face and roadway in the mining panel.

During the mining of an extrathick coal seam under hard roofs, due to the large mining thickness, the migration range of overburden is wide. The results showed that the failure height could reach 200 to 350 m during a 14 to 20 m-thick coal seam mining [10–12]. Field monitoring showed that

the fracturing of hard roofs in a large space frequently resulted in the occurrence of ground pressure on the working face with a different strength and manifestation [13, 14]. The ground pressure on the working face shows the characteristics of “long and short duration”, of which the “long duration” interval was 30 to 60 m and the “short duration” interval was 12 to 20 m, the pressure intensity increased when the “long duration” occurred. However, there was no obvious regularity in the occurrence of strong ground pressure such as support failure or severe roadway deformation [15, 16]. Li et al. [17] found that the huge mining thickness of an extrathick coal seam results in a larger mobile space of high-level hard roofs, and the sliding instability of the high-level hard roofs would cause strong ground pressure. Singh et al. [18] studied the strata movement during underground mining of a thick coal seam. According to Li et al.’s research [19], the rotational movement of key strata in the overburden had a direct impact on the supports in the working face, and the dynamic loading induced by the instability of the Vossior beam structure was analyzed. Xie and Xu [20] analyzed the influence law of different thickness and level of hard roofs on the peak value and influencing range of the abutment stress. Yu et al. and Chen et al. conducted field measurement on the deformation characteristics and stress distribution law of a roadway in the process of mining an extrathick coal seam under hard roofs [21, 22]. Guo et al. [23] studied the relationship between the support resistance and the overhanging distance of hard roofs, and criteria for reasonable selection of support resistance were given. Mondal et al. [24] monitored the strata behavior in the destressed zone of a shallow Indian longwall panel with hard sandstone cover using mine-microseismicity and borehole televiewer data. However, other scholars also invest in the hard roof research [25, 26]; the results show that the occurrence of the hard roof has a direct impact on the ground pressure in the working face and is complex.

In terms of the mining conditions of extrathick coal seams with hard roofs, failure and instability of hard roofs will occur gradually within a large space, which may further result in frequent occurrence of ground pressure of different strengths on the working face. Most of the aforementioned scholars focused on the structural characteristics of the overburden or worked from the perspective of mining pressure development but did not do in-depth research on the mechanism of ground pressure induced by the fracturing of hard roofs at different levels. According to the key stratum theory [27, 28], the lower level key stratum is close to the coal seam, and the breaking span is small. With increase in the occurrence level, the breaking span and the strength of the high-level key stratum increase accordingly. Therefore, due to the influence of the distance from the coal seam and the breaking span, the failure and instability of key strata at the low and high levels may have different effects on the ground pressure. In addition, the large breaking span and instability of high-level hard roofs may cause the occurrence of strong ground pressure on the working face and could have interaction with the lower key layers. A physical simulation experiment could reflect the structural characteristics of the overburden and its influence on the abutment stress of a min-

ing panel directly and was considered an effective means to study the overburden structure and ground pressure in coal seam mining [29, 30]. Based on the exploitation of extrathick coal seams with hard roofs, for this paper, the research method of physical simulation was adopted to study the fracture law of key strata and the strength of ground pressure induced by the breakage and instability of strata in different levels.

2. Experimental Model

2.1. Geological Background. The carboniferous #3–5 extrathick coal seams were mainly mined in Tashan coal mine of the Datong mining area, with a thickness of 14 to 20 m. The method of top coal caving mining was adopted. The buried depth of the coal seam is 400 to 800 m, and the overburden is covered with multilayer hard roofs with the compressive strength of 60 to 120 MPa. Due to the large mining thickness of the coal seam, the fracturing of multiple layers in a large space resulted in a frequently strong ground pressure, accompanied by the supports crashed. The floor heave was severe within 10 to 40 m in advanced roadway, and the maximum floor heave was up to 0.8 m. The roof subsidence was up to 0.6 m, the shotcrete of the two sides of the roadway was seriously cracked, and the advanced individual props were seriously damaged, as shown in Figure 1.

Taking the #8216 working face in Tashan coal mine as an example, the Carboniferous #3–5 coal seam was mined, the average thickness of the coal seam was 16 m, and the buried depth and inclination of the coal seam was 418 to 522 m and 1 to 3°, respectively. The length and mining distance of the working face was 230 and 1500 m, respectively, and the coal seam was covered with multiple hard roofs.

Based on the statistics of the strong ground pressure during the mining process, as shown in Table 1, it can be found that the pressure on the working face was relatively strong within the initial mining range of 214 m. The roadway deformation and hydraulic props collapsed were serious in advanced 35 m, the support resistance increased obviously and was even accompanied by safety valve opening. In the later mining process, the strength of the ground pressure was relatively weakened, the influence range was reduced to 10 m in an advanced roadway, and the deformation was also reduced.

2.2. Basic Parameters of the Model. In order to study the effect of key stratum fracturing on the ground pressure in the working face, the method of physical simulation was used in the laboratory. Taking the #8101 working face as the background, the Carboniferous #3–5 coal seam was mined. The thickness and burial depth of the coal seam was 20 and 470 m, respectively. The coal seam dip was 1 to 3°, and the length and mining distance of the working face was 230 and 1500 m, respectively. The frame size of the physical model in the laboratory was 2.5 × 0.2 × 1.9 m (length × width × height). The geometric similitude ratio of the designed model was 150 : 1; the actual height of the model was 1.47 m, which simulated a height of 220 m. Materials including sand, calcium carbonate, and gypsum were used

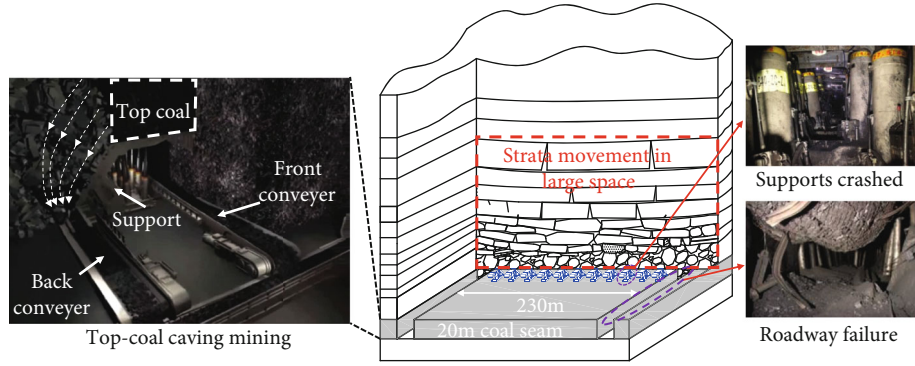


FIGURE 1: Caving mining method and strong ground pressure in the working face.

TABLE 1: Statistics of the strong ground pressure on the working face.

| Data | Mining distance (m) | Phenomenal description |
|------------|---------------------|---|
| 2015.11.13 | 110.2 | Strong ground pressure 10 m in advance of the working face, the floor heave was 0.3–0.4 m, rib heave was serious: 0.4 m; the resistance of supports #45 to #67 was high. |
| 2015.11.21 | 168.8 | A stronger ground pressure happened, the advanced range of influence was 10–20 m, roof subsidence and floor heave was severe, ten hydraulic props were dumped, roof subsidence 0.3–0.4 m, floor heave 0.45 m, the resistance of supports #23 to #35 and #56 to #71 were high. |
| 2015.12.30 | 214.5 | A stronger ground pressure occurred 12–35 m in advance of the roadway, thirty hydraulic props were dumped; the roadway deformation in horizontal and vertical direction was 0.5 and 0.8 m, respectively. The resistances of supports in the working face were all higher and the safety valves opened at supports #45 to #67. |
| 2016.1.14 | 450.0 | Strong pressure happened 10 m in advance of the working face, an obvious deformation occurred in the roadway, one hydraulic prop was bent 8 m in advance working face; the resistance of supports increased obviously. |
| 2016.2.13 | 635.0 | Ground pressure occurred, the pressure was concentrated 10 m in advance, the floor heave was 0.2–0.3 m, and roof subsidence was not obvious. |
| 2016.3.18 | 736.0 | Ground pressure occurred. At 15 m in advance, the floor heave was 0.2–0.4 m, rib heave and roof subsidence were not obvious, and five props inclined. |

TABLE 2: Basic parameters of the physical similarity model.

| Items | Parameters | Items | Parameters |
|---------------------|------------|------------------------|--------------|
| Length of model | 2.5 m | Mining distance | 2.1 m |
| Thickness of model | 0.2 m | Model boundary | 10 cm |
| Height of model | 1.47 m | Excavation steps | 45 |
| Coal seam thickness | 13.3 cm | Excavate distance once | 5 cm |
| Geometric ratio | 150 : 1 | Excavate time interval | 0.5 h |
| Weight ratio | 1.667 : 1 | Excavation time | 21 h |
| Stress ratio | 250 : 1 | Compensation stress | 0.027265 MPa |

to simulate the overlying rock. The weight ratio, time ratio, and stress ratio were 1.667 : 1, 12.25 : 1, and 250 : 1, respectively. The actual working time of the working face is 16 hours per day, and the maintenance work time is 8 hours. The advanced distance is about 4 m per day. Therefore, the actual working time and excavation distance on the model can be calculated to be every 78 min and 2.6 cm each time. The thickness of the overlying unladen strata was 272.65 m; then, the weight of the overburden rock is 6.816 MPa, and the magnitude of the compensation stress added to the upper

part of the similar model is 0.027265 MPa. The basic parameters of the model are shown in Table 2.

Table 3 shows the physical and mechanical parameters of the coal and rock mass [31]. According to the similarity ratio, the matching parameters of each rock formation in the model are shown in Table 3. The rock layers No.32, No.27, No.22, No.16, and No.9 above the coal seam are calculated to be the key strata based on the key stratum theory [27, 28], which are the emphasis to be studied in this test.

TABLE 3: Parameters of the coal and rock.

| No. | Lithology | Depth (m) | Thickness (m) | Simulated thickness (cm) | Compression strength (MPa) | Simulated strength (KPa) | Matching number | Weight (kg) | Sand (kg) | Calcium carbonate (kg) | Gypsum (kg) | Water (kg) |
|-----|------------------|-----------|---------------|--------------------------|----------------------------|--------------------------|-----------------|-------------|-----------|------------------------|-------------|------------|
| 1 | Gritstone | 267.01 | 4.9 | 3.3 | 28.34 | 113.36 | 373 | 29.4 | 22.05 | 5.15 | 1.65 | 4.20 |
| 2 | Packsand | 271.91 | 12.1 | 8.1 | 90.53 | 362.12 | 437 | 72.6 | 58.08 | 4.36 | 8.13 | 8.07 |
| 3 | Siltite | 284.01 | 3.7 | 2.5 | 33.6 | 134.4 | 737 | 22.2 | 19.43 | 0.83 | 1.70 | 2.47 |
| 4 | Gritstone | 287.71 | 2.8 | 1.9 | 23.1 | 92.4 | 473 | 16.8 | 13.44 | 2.35 | 0.81 | 1.87 |
| 5 | Pebblestone | 290.51 | 4.5 | 3.0 | 35.6 | 142.4 | 555 | 27 | 22.50 | 2.25 | 1.88 | 3.00 |
| 6 | Gritstone | 295.01 | 5 | 3.3 | 25.9 | 103.6 | 755 | 30 | 26.25 | 1.88 | 1.64 | 3.33 |
| 7 | Conglomerate | 300.01 | 5 | 3.3 | 37.74 | 150.96 | 455 | 30 | 24.00 | 3.00 | 2.40 | 3.33 |
| 8 | Siltite | 305.01 | 5 | 3.3 | 24.1 | 96.4 | 473 | 30 | 24.00 | 4.20 | 1.44 | 3.33 |
| 9 | Packsand | 310.01 | 12.9 | 8.6 | 80.21 | 320.84 | 337 | 77.4 | 58.05 | 5.81 | 10.16 | 11.06 |
| 10 | Gritstone | 322.91 | 5 | 3.3 | 26.6 | 106.4 | 755 | 30 | 26.25 | 1.88 | 1.64 | 3.33 |
| 11 | Medium sandstone | 327.91 | 4.8 | 3.2 | 30.3 | 121.2 | 655 | 28.8 | 24.69 | 2.06 | 1.76 | 3.20 |
| 12 | Siltite | 332.71 | 3 | 2.0 | 35.87 | 143.48 | 555 | 18 | 15.00 | 1.50 | 1.25 | 2.00 |
| 13 | Conglomerate | 335.71 | 5.2 | 3.5 | 25.6 | 102.4 | 755 | 31.2 | 27.30 | 1.95 | 1.71 | 3.47 |
| 14 | Pebblestone | 340.91 | 5.4 | 3.6 | 32.3 | 129.2 | 737 | 32.4 | 28.35 | 1.22 | 2.48 | 3.60 |
| 15 | Siltite | 346.31 | 4 | 2.7 | 23.57 | 94.28 | 473 | 24 | 19.20 | 3.36 | 1.15 | 2.67 |
| 16 | Packsand | 350.31 | 12.2 | 8.1 | 80.27 | 321.08 | 337 | 73.2 | 54.90 | 5.49 | 9.61 | 10.46 |
| 17 | Gritstone | 362.51 | 5.7 | 3.8 | 32.87 | 131.48 | 737 | 34.2 | 29.93 | 1.28 | 2.62 | 3.80 |
| 18 | Conglomerate | 368.21 | 3.3 | 2.2 | 22.9 | 91.6 | 473 | 19.8 | 15.84 | 2.77 | 0.95 | 2.20 |
| 19 | Siltite | 371.51 | 3 | 2.0 | 33.85 | 135.4 | 737 | 18 | 15.75 | 0.68 | 1.38 | 2.00 |
| 20 | Medium sandstone | 374.51 | 4.83 | 3.2 | 30.24 | 120.96 | 655 | 28.98 | 24.84 | 2.07 | 1.77 | 3.22 |
| 21 | Siltite | 379.34 | 5 | 3.3 | 23.23 | 92.92 | 473 | 30 | 24.00 | 4.20 | 1.44 | 3.33 |
| 22 | Packsand | 384.34 | 10.12 | 6.7 | 65.53 | 262.12 | 337 | 60.72 | 45.54 | 4.55 | 7.97 | 8.67 |
| 23 | Pebblestone | 394.46 | 5.6 | 3.7 | 30.23 | 120.92 | 373 | 33.6 | 25.20 | 5.88 | 1.89 | 4.80 |
| 24 | Mudstone | 400.06 | 5.8 | 3.9 | 25.3 | 101.2 | 755 | 34.8 | 30.45 | 2.18 | 1.90 | 3.87 |
| 25 | Conglomerate | 405.86 | 3.8 | 2.5 | 29.13 | 116.52 | 373 | 22.8 | 17.10 | 3.99 | 1.28 | 3.26 |
| 26 | Siltite | 409.66 | 5.25 | 3.5 | 36.56 | 146.24 | 555 | 31.5 | 26.25 | 2.63 | 2.19 | 3.50 |
| 27 | Packsand | 414.91 | 9.1 | 6.1 | 55 | 220 | 437 | 54.6 | 43.68 | 3.28 | 6.12 | 6.07 |
| 28 | Siltite | 424.01 | 6.4 | 4.3 | 30.73 | 122.92 | 655 | 38.4 | 32.91 | 2.74 | 2.35 | 4.27 |
| 29 | Conglomerate | 430.41 | 3.2 | 2.1 | 23.6 | 94.4 | 473 | 19.2 | 15.36 | 2.69 | 0.92 | 2.13 |
| 30 | Medium sandstone | 433.61 | 4 | 2.7 | 30.43 | 121.72 | 655 | 24 | 20.57 | 1.71 | 1.47 | 2.67 |
| 31 | Gritstone | 437.61 | 5.05 | 3.4 | 38.6 | 154.4 | 455 | 30.3 | 24.24 | 3.03 | 2.42 | 3.37 |
| 32 | Packsand | 442.66 | 9.44 | 6.3 | 55.53 | 222.12 | 437 | 56.64 | 45.31 | 3.40 | 6.34 | 6.29 |

TABLE 3: Continued.

| No. | Lithology | Depth (m) | Thickness (m) | Simulated thickness (cm) | Compression strength (MPa) | Simulated strength (KPa) | Matching number | Weight (kg) | Sand (kg) | Calcium carbonate (kg) | Gypsum (kg) | Water (kg) |
|-----|----------------|-----------|---------------|--------------------------|----------------------------|--------------------------|-----------------|-------------|-----------|------------------------|-------------|------------|
| 33 | Sandy mudstone | 452.1 | 5.65 | 3.8 | 33.3 | 133.2 | 737 | 33.9 | 29.66 | 1.27 | 2.60 | 3.77 |
| 34 | Conglomerate | 457.75 | 3.2 | 2.1 | 23.34 | 93.36 | 473 | 19.2 | 15.36 | 2.69 | 0.92 | 2.13 |
| 35 | Siltstone | 460.95 | 4.5 | 2.9 | 21.07 | 84.28 | 573 | 26.4 | 22.00 | 3.08 | 1.10 | 2.93 |
| 36 | Mudstone | 465.35 | 4.3 | 2.9 | 17.36 | 69.44 | 773 | 25.8 | 22.58 | 2.26 | 0.85 | 2.87 |
| 37 | #3-5 coal seam | 469.65 | 20 | 13.3 | 15.94 | 63.76 | 773 | 120 | 105.00 | 10.50 | 3.94 | 13.33 |
| 38 | Gritstone | 489.65 | 3 | 2.0 | 43.87 | 175.48 | 637 | 18 | 15.43 | 0.77 | 1.54 | 2.00 |

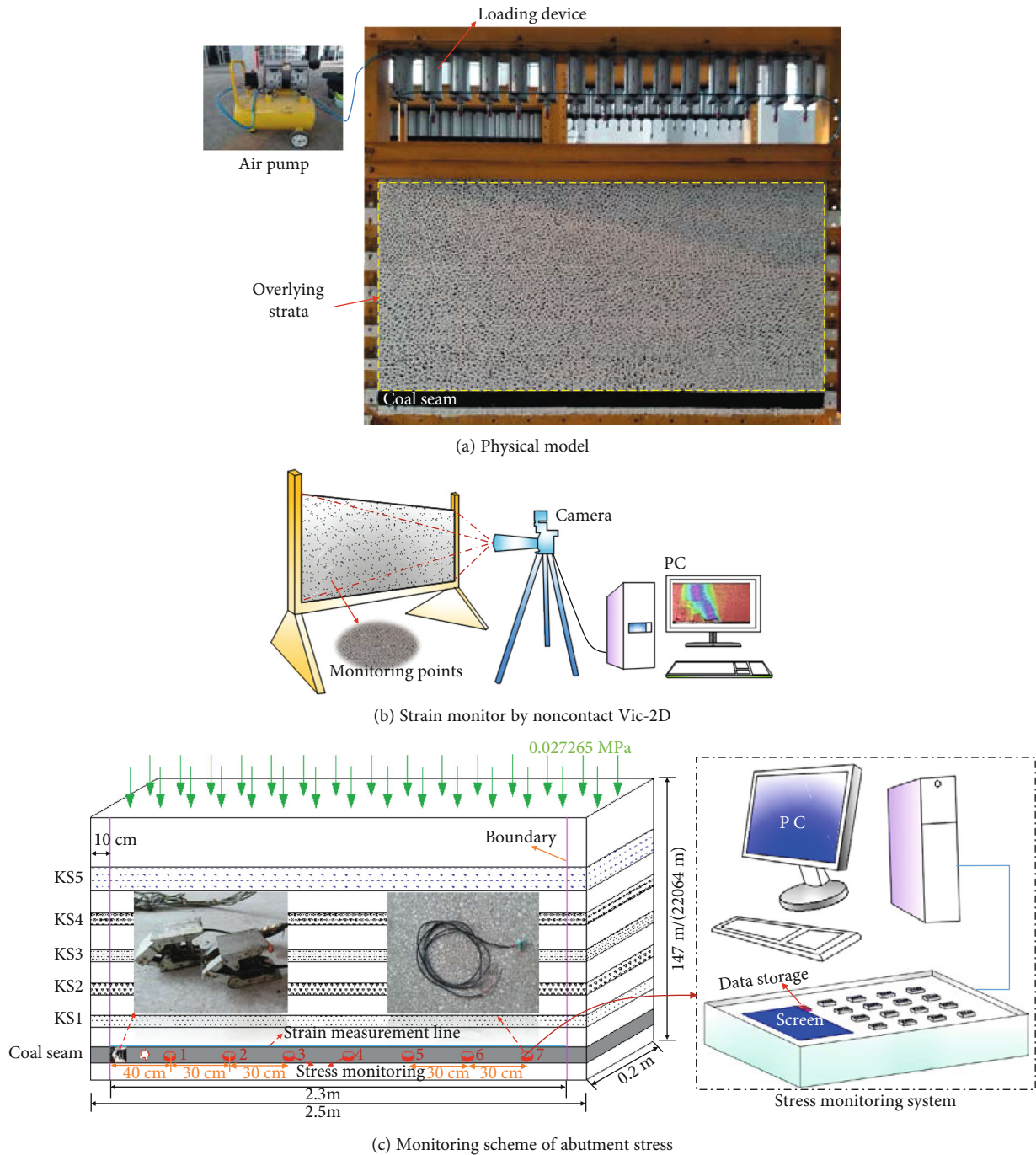
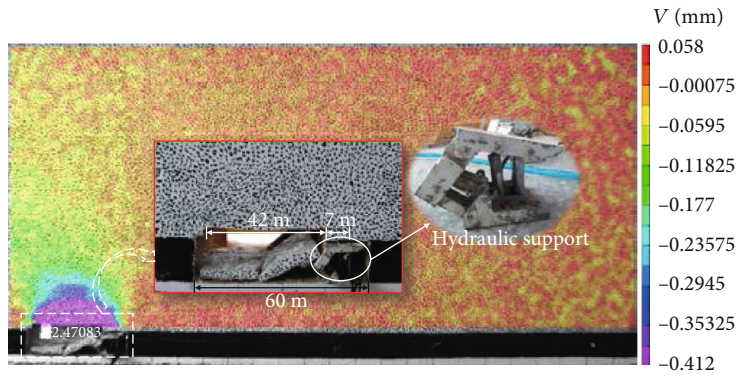


FIGURE 2: Monitoring system of the physical model.

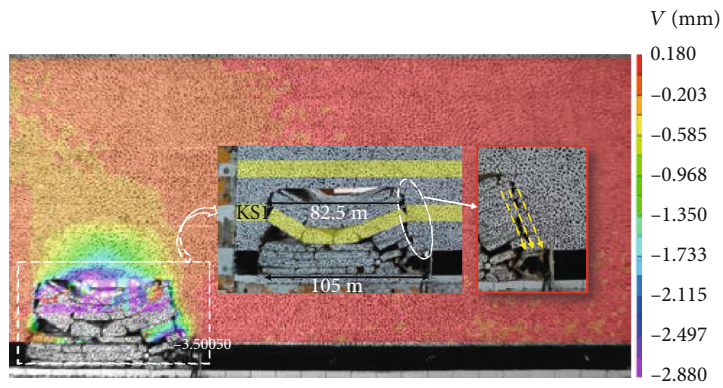
2.3. Monitoring System. The monitoring system schematic is shown in Figure 2. Taking five key strata as the research objects (17, 45, 75, 107, and 146 m vertically above the coal seam), the thickness of each key layer was 9.44, 9.1, 10.12, 12.2, and 12.9 m, respectively. In order to monitor the influence of each key layer breaking on the distribution characteristics of the abutment stress in the coal body, a total of seven strain monitors were arranged at intervals of 30 cm in the coal seam. The first measurement point was 40 cm from the open-off cut of the working face. In order to truly reflect

the structural characteristics of the overburden, a small simulated hydraulic support was placed on the working face.

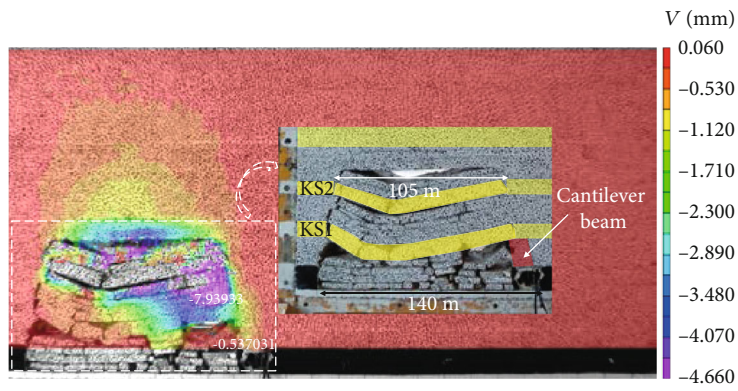
A noncontact strain monitoring system (Vic-2D) was used to monitor the overburden displacement timely, as seen in Figure 2(b). Black flecks were randomly sprayed onto the model surface, and a camera was used to capture movement of the flecks in real time as the overburden moved. The displacement of the flecks was obtained by postprocessing software and was inverted to the displacement-changes law of the overlying strata.



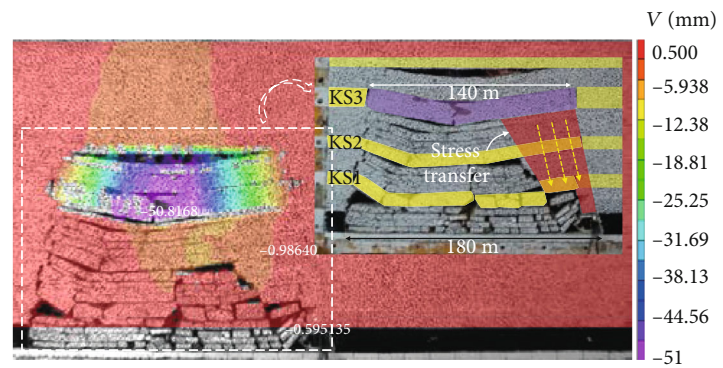
(a) Fracturing of immediate roof



(b) Fracturing of KS1

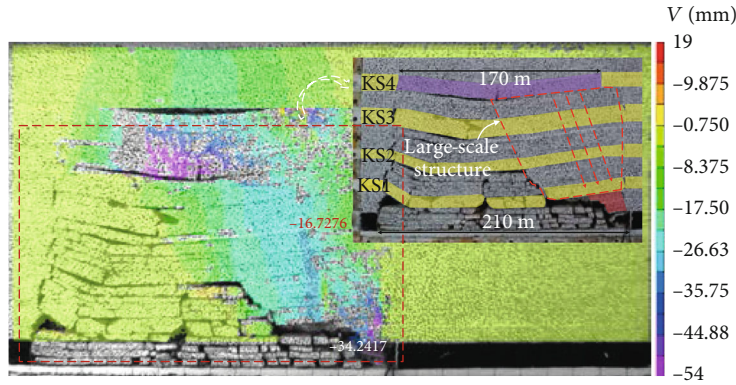


(c) Fracturing of KS2

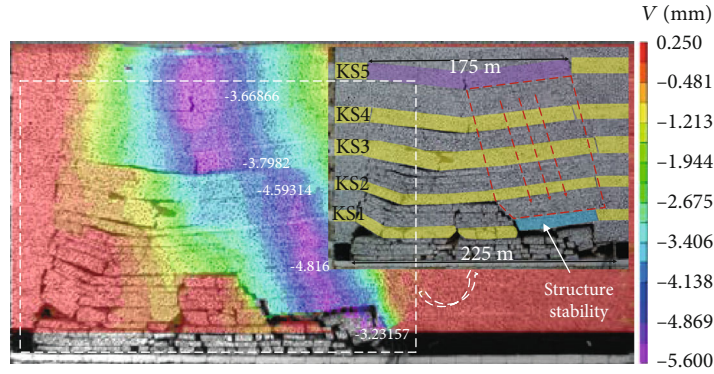


(d) Fracturing of KS3

FIGURE 3: Continued.



(e) Fracturing of KS4



(f) Fracturing of KS5

FIGURE 3: Structure and displacements during the fracturing of strata at different levels.

TABLE 4: The calculated elasticity modulus of strain gauges.

| No. | Weight P (N) | Strain ε (10^{-3}) | Elasticity modulus E (GPa) |
|------|----------------|------------------------------------|------------------------------|
| 1 | 32 | 210 | 0.121322414 |
| | 64.4 | 412 | 0.124451178 |
| 2 | 32 | 230 | 0.110772639 |
| | 64.4 | 428 | 0.119798798 |
| 3 | 32 | 330 | 0.077205173 |
| | 64.4 | 540 | 0.09495164 |
| 4 | 32 | 290 | 0.087854162 |
| | 64.4 | 690 | 0.074309979 |
| Avg. | | | 0.101333248 |

3. Analysis of Experimental Results

3.1. Structural Characteristics of the Overlying Strata. The mined interval of the simulated working face was 5 cm every 30 minutes. The structural characteristics and overburden displacement variation during hard roof fracturing at different levels were obtained, as shown in Figure 3.

When the working face was mined 60 m, the roof broke for the first time, with a breaking span of 42 m. The length of the broken block above the support was 7 m, and its weight was borne by the support. After the roof broke for the first

time, the overlying unbroken strata flexed and sank by 20 cm, as shown in Figure 3(a).

When the working face was mined for 105 m, KS1 broke for the first time, with a breaking span of 82.5 m. The fracturing of KS1 caused synchronous rotation and collapse of lower strata and resulted in vertical variation of 0.42 m in the support. This increased the working resistance of the support, as shown in Figure 3(a).

When the working face was mined for 140 m, KS2 broke for the first time, and the initial fracturing step of KS2 was up to 105 m. The fracturing of KS2 caused synchronous failure and instability of the underlying strata, resulting in rotary movement, as shown in Figure 3(c). The intension was low during the KS2 breakage and the KS1 structure remained stable, which reduced the strength of the KS2 breakage. According to Figure 3(c), we could see that the vertical displacement of the support was only 0.22 m and the rock layer above the support showed the structural characteristics of a composite cantilever beam.

When the working face was mined 180 m, KS3 broke for the first time, with a breaking span of 140 m and a rotary subsidence of 7.5 m. The thickness of KS3 was 10.12 m. Due to its large thickness, breaking span, and rotary subsidence, the energy release intensity was relatively high during the breakage of KS3, thus resulting in synchronous rotary movement of the underlying strata. As shown in Figure 3(d), the drop-off in the support reached 0.9 m.

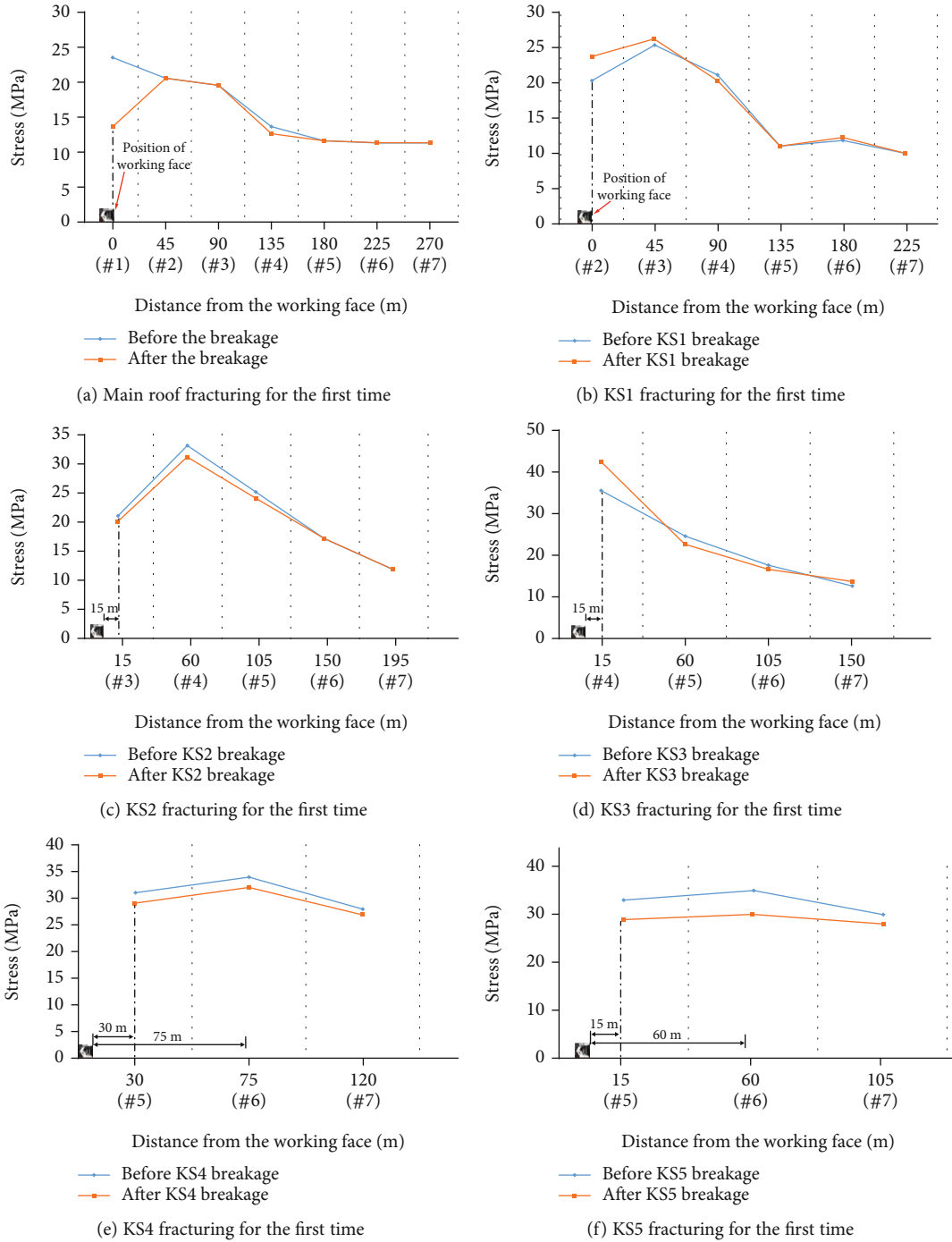


FIGURE 4: Stress distribution during the overburden fracturing.

When the working face was mined to 210 m, KS4 in the high and far field broke for the first time. The breaking step distance was up to 170 m and the thickness of KS4 was 12.2 m. The high intensity of the KS4 fracturing resulted in the synchronous rotation of KS1, KS2, and KS3. The rotary movement of this large rock structure acted on the cantilever beam structure above the support, resulting in a 2.5 m vertical displacement of the cantilever beam structure and intense pressure on the support, as shown in Figure 3(e).

When the working face was mined for 225 m, KS5 broke for the first time. The breaking step distance was 175 m, and the thickness of KS5 was 12.9 m. In the case of the KS5 fracturing, although the intensity was relatively high, due to its long distance from the coal seam, the fracturing of KS5 did not cause instability rotation in all the underlying strata. As shown in Figure 3(f), the cantilever structure of KS1 maintained its own stability, thus having a certain protective effect on the working face. However, due to the high breaking

TABLE 5: Range of stress influence before and after strata fracturing.

| | Before breaking | | After breaking | |
|-----|-------------------|---------------------|------------------|------------------------|
| | Peak stress (MPa) | Influence range (m) | Action range (m) | Stress variation (MPa) |
| KS1 | 30 | 45 | > 0 | 24 → 28 |
| KS2 | 33 | 60 | < 15 | — |
| KS3 | 25 | 60 | > 15 | 36 → 43 |
| KS4 | 34 | 120 | < 30 | — |
| KS5 | 33 | 105 | > 15 | — |

intensity of KS5, the vertical displacement at the immediate roof was still up to 0.48 m, and the breaking impact on the support was slightly lower than that of KS4.

Based on the comprehensive analysis of the overlying strata fracturing, it was found that due to the large mining thickness of the coal seam and the wide range of overlying rock migration, the key strata of KS1 to KS5 all broke, and the key strata at different levels had different influences on the working face. The fracturing of KS1 and KS2 in the near field formed a cantilever beam and masonry beam structure, which resulted in a slight ground pressure on the working face. When the far field KS4 broke, due to its great thickness and wide breaking span of 170 m, the ground pressure on the working face was most intense. The intension of the KS5 fracturing was also high with a breaking span of 175 m, but due to the long distance from the coal seam and the stable structure in the lower strata, the effects of KS5 fracturing on the working face was reduced compared to KS4, and the working face showed slightly strong ground pressure.

3.2. Variation of Abutment Stress in the Coal Body. The above analysis was made based on the overburden structural characteristics and displacements when the key strata broke at different layers. The influence of the occurrence and fracturing of key strata on the stress distribution in the coal body could be gained based on the monitored strain value; the calculation process is shown in the following. The strain gauges in the coal seam were numbered 1-7 along the mining direction of the working face, as shown in Figure 2(c). Four strain gauges were selected to decide the elasticity modulus, as shown in Table 4. Thus, based on the elasticity modulus and monitored strain, the stress variation at each monitor point were gained, as shown in Figure 4.

The abutment stress distribution during the first fracturing of the main roof is shown in Figure 4(a), where the No.1 monitoring point is next to the working face. After the main roof breaks, the stress at the No.1 monitoring point decreases from 24 to 14 MPa, indicating that the stress concentration on the coal wall is reduced to a certain extent. When KS1 broke for the first time, the No.2 monitoring point is close to the working face. Due to the rotation of KS1, the stress at the coal wall increases from 24 to 28 MPa, as shown in Figure 4(b). During the first breaking of KS2, the No.3 monitoring point is 15 m from the working face, and the strata fracturing has little impact on the abutment stress, as shown in Figure 4(c). When KS3 first broke, the No.4 monitoring point is 15 m from the working face. As a result of KS3 break-

ing, the stress value at No.4 monitoring point increases from 36 to 43 MPa. Meanwhile, at monitoring points No.5 and No.6, the stress decreases slightly, as shown in Figure 4(d), indicating that the stress concentration in the advanced 60 m is reduced. When KS4 breaks, monitoring points No.5 and No.6 are 30 m and 75 m, respectively, away from the working face. The stress values at monitoring points #5 and #6 are reduced from 31 and 34 MPa to 29 and 32 MPa, respectively, as shown in Figure 4(e). When KS5 broke for the first time, monitoring points No.5 and No.6 is 15 m and 60 m, respectively, away from the working face. The stress change law is similar to that for KS4, as shown in Figure 4(f).

The influence of hard roof fracturing at different layers on the peak stress and the range of the abutment stress in the advanced coal body were obtained statistically (see Table 5).

As shown in Table 5, with the development of the overburden caving height, the abutment stress and the influence range in advanced coal seam increase accordingly. The peak stress in the advanced coal body increases slightly (30 to 34 MPa), and the advanced range of influence increases greatly. Before the critical fracturing of KS4, the range of influence of the advanced abutment stress reaches 120 m.

When the key strata broke, the strata rotations squeezed the coal body near the working face, causing the stress on the coal body to rise. Affected by the strain monitoring layout interval, it was impossible to accurately calculate the range of influence in the advanced coal body affected by the fracturing of each key layer, but we could still find from Table 5 that the fracturing of KS4 resulted in a strong compression zone of 15–30 m in advance of the working face. With the increase of the distance between the key stratum and coal seam, the buffer action of the underlying strata was strengthened, and the strong compression area in the advanced coal body was weakened accordingly (e.g., KS5). As the distance between the key stratum and the coal seam decreased, the breaking span and the range of the advanced compression zone decreased accordingly (e.g., KS3).

3.3. The Advanced Failure Zone. Based on the noncontact strain monitoring system, the strain variation characteristics of the advanced coal body were gained through the strain measurement line to further study the range and degree of influence on strong compression areas caused by the fracturing of each key layer.

Strain measurement lines were arranged at the interface of the coal seam and immediate roof to obtain strain variation of the coal body after the fracturing of KS1 to KS5, as shown in Figure 2; the results are shown in Figure 5. The abscissa represents the location of monitoring points along the mining direction, the leftmost side of the model is the coordinate zero point, and the coordinate axis increases along the mining direction of the working face accordingly. The length of the model is 375 m.

The boundary pillar of 15 m was retained in the model. When the working face was mined to 105 (corresponds to abscissa $x = 120$ m), KS1 broke, and a statistical strain curve of the coal body before and after KS1 was obtained, as shown

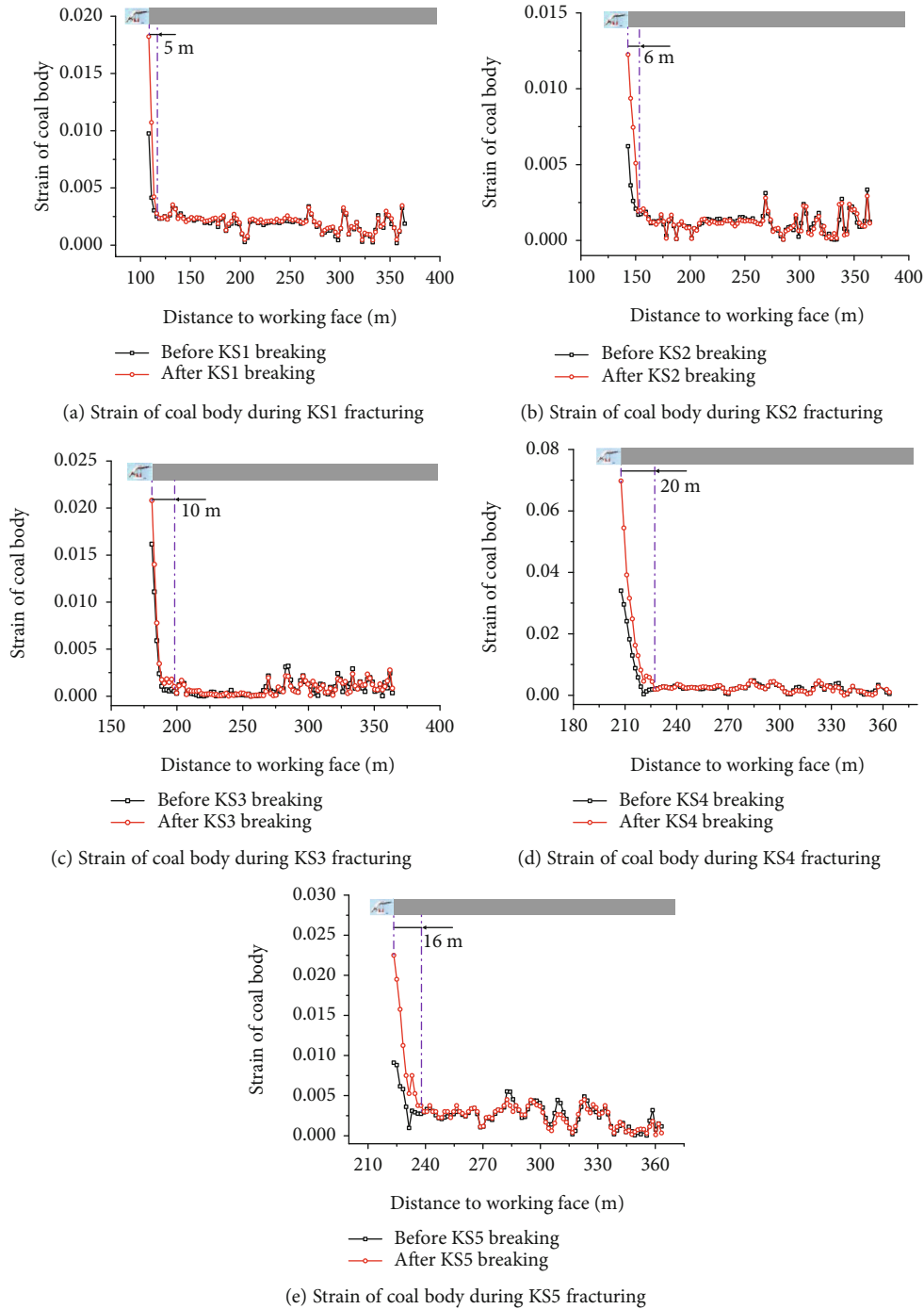


FIGURE 5: Strain of coal body during fracturing of different key strata.

in Figure 5(a). The simulated support is 15 m long. From Figure 5(a), we can find that the coal body is compressed in the advanced 5 m, that is, the impact range of the KS1 fracturing on the advanced coal body is about 5 m. Similarly, the strain curve during KS2 fracturing is obtained as shown in Figure 5(b). Compared with KS1, the compressed zone in the advanced coal body caused by KS2 fracturing slightly increases, reaching 6 m. As shown in Figure 5(c), the compressed range in the advanced coal body during the fracturing of KS3 reaches 10 m. According to the coal body failure

criterion obtained from the test, the fracturing of KS3 resulted in 3 m of advanced coal body failure.

When KS4 broke, due to its high breaking strength and strong impact, the strain on the coal body was greatly increased, as shown in Figure 5(d). The maximum strain variable in the advanced coal body is up to 0.07, which could easily cause the crash of supports and the advanced influence range of 20 m. The coal body is severely compressed in the advanced 20 m. Similar to KS4, the action of KS5 fracturing on the advanced coal body is also relatively serious, but the

range of influence and action intensity are lower than that of KS4, as shown in Figure 5(e). The range of influence from the KS5 fracturing on the advanced coal body is 16 m.

4. Discussion

According to Figure 5, the range of influence and degree of overburden-key-strata fracturing in the advanced coal body are statistically obtained as shown in Figure 6. It can be seen from Figure 6 that, with an increase of the occurrence level of key strata, the impact strength of each key layer fracturing on the coal body increases accordingly. The fracturing of KS4 has the strongest effect on the advanced coal body, with the maximum strain variation of the coal body reaching 0.036 and the influence range reaching 20 m. With further increase of the distance between the key layer and the coal seam, taking KS5 as an example, the action strength of KS5 on the advanced coal body decreases, the change of strain on the coal body is 0.013, and the range of influence decreases to 16 m. As the distance between the key strata and the coal seam gets closer, the intensity of the key strata fracturing will also decrease due to decrease of the breaking span of the key strata. Taking KS3 as an example, the maximum change in the strain on the advanced coal body caused by the KS3 fracturing is 0.005, and the range of influence is 10 m.

Combined with the above studies, we can find that the impact strength of the fracturing of key strata on the mining panel pressure is directly related to the breaking span, occurrence location, and distribution of the underlying strata. The physical simulation studies show that KS4 fracturing had the strongest effect on the mining panel pressure, followed by KS5. The ratio of the distance between KS4 and KS5 from the coal seam and the coal seam thickness are 5.35:1 and 7.3:1, respectively.

From Figure 6, we can see that the compression induced in the coal body by the fracturing of KS4 and KS5 are greater than that of KS1–KS3. This is mainly because during the fracturing of KS1 to KS3, the lower bed-separation space and key layer rotation angle are big. Although the impact velocity of the key strata is larger, the breaking step of key strata is relatively small. In addition, the key strata are more likely to act on the goaf caved rock mass, as shown in Figure 7(a), which has a weak impact on the mining panel pressure.

As the overburden fracture height develops, the bed-separation space under the far field key strata decreases, and the impact velocity after the breaking of key strata decreases accordingly. However, the kinetic energy after a far field key strata break is huge due to its great thickness, high strength, and large breaking interval, coupled with small rotary space. The kinetic energy of strata fracturing mostly acts on the lower overburden, resulting in a synchronous rotary movement of the lower overburden rock strata. This causes strong ground pressure in the advanced coal body and working face, as shown in Figure 7(b).

With further increase of the vertical distance between the key strata and the coal seam, the bed-separation space is further reduced, and the energy transferred from the key strata fracturing to the coal seam is weakened accordingly. Strata fracturing does not necessarily cause instability and synchro-

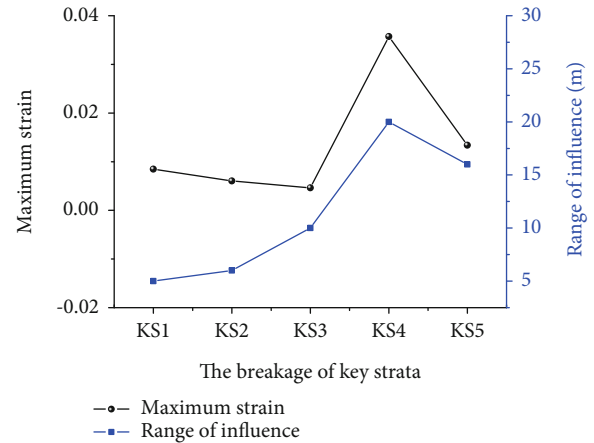


FIGURE 6: Effect on the coal body of fracturing of different levels of hard strata.

nous movement of the underlying strata. According to the above physical simulation analysis, in this geological condition, the KS4 fracturing (in the far field) has the most serious impact on the working face, followed by KS5. The vertical distance from the coal seam of KS4 and KS5 are 107 and 146 m, respectively, and the ratio of the vertical distance to the coal-seam thickness is 5.35 and 7.3, respectively.

At the same time, we also used the method of field measurement to study the ground pressure in the mining of extrathick coal seams with hard roofs [13, 15]. The thickness of the coal seam was 19 m, and the method of top coal caving mining was adopted. The strata movement measurement points were arranged in key strata at different levels (22, 51, and 104 m away from the coal seam). The thickness of the three key strata was 12, 9.8, and 23 m from the bottom up. Meanwhile, the resistance characteristics of the working face support were recorded in real time, as shown in Figure 8. The monitoring results showed that the support resistance in the working face increased with fracturing of the two key strata, which were 22 and 51 m away from the coal seam at the low level, and the dynamic load coefficient of the support was 1.15 and 1.34, respectively. The pressure duration was 7 h and 16 h, respectively, and the working face had no obvious indications of strong ground pressure. When the 23 m-thick key layer (which was 104 m from the coal seam) broke, the #35–95 supports in the working face were crushed, and the dynamic load coefficient of the supports reached 1.54. The pressure duration reached 43 h, and the ratio of the distance between the highest key layer and the coal seam, to the coal seam thickness, was 5.47.

Thus, due to the great thickness of the extrathick coal seam, the range of the overburden movement was huge and the key strata at all different levels broke. Among them, the hard roof in the far field had the largest breaking span and highest energy intensity. This resulted in the synchronous rotation of the underlying strata, which is the main reason of the occurrence of strong ground pressure on the working face. Based on the above studies, it was found that thick, hard strata, with the ratio of the distance from the coal seam to the coal seam thickness between 5.3 and 7.3, have the most

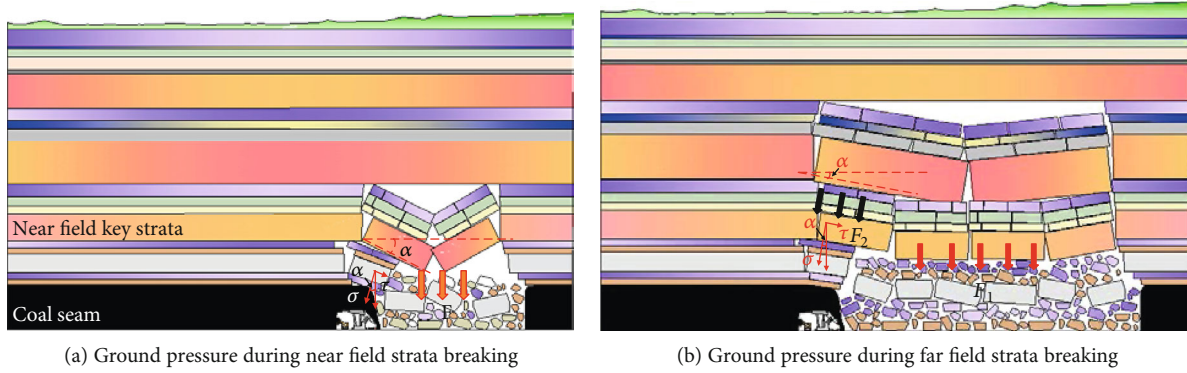


FIGURE 7: Ground pressure during the breaking of strata at different levels.

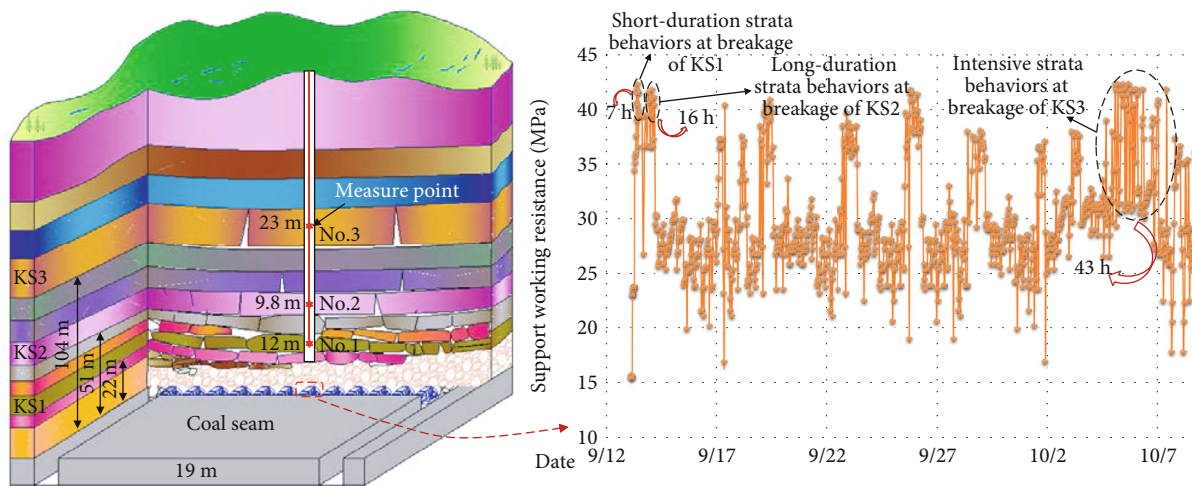


FIGURE 8: Ground pressure during the breaking of strata at different levels.

serious impact on the working face. That is, when a 20 m-thick coal seam is mined, the thick and hard roof, which is within the range of 106 m to 146 m away from the coal seam, has the greatest impact on the mining pressure of the working face. The results provide a theoretical basis for guiding the selection of the hard roof control layer in a large space and improve the reliability of the hard roof control. The results show that the high-level hard strata are the main factor causing strong ground pressure in the stope, which breaks through our idea of control ground pressure by low-level rock weakening and improves the reliability and accuracy of ground pressure control. For the control of high-level hard strata, traditional technical means cannot reach that height. Thus, our team developed a technical method of ground fracturing to control high-level hard strata and achieved success. This will be introduced in the follow-up researches.

5. Conclusions

- (1) Based on physical simulation criterion, a physical model for the mining of an extrathick coal seam with hard roofs was established and the methods of non-contact strain monitor and abutment stress monitoring were used to study the structure characteristics

and the corresponding ground pressure of hard roofs at different levels

- (2) The research showed that the lower key strata mostly collapse into goaf, thus having less impact on the working face and advanced coal body. During the thick, hard key stratum in the far field breaking, the large fracturing span and high strength result in instability and synchronous rotation of the underlying strata, thus causing the supports crashed and advanced coal body damaged, which is the main reason for the occurrence of strong ground pressure
- (3) Combined with the physical simulation and field measurement studies, it is found that the characteristics of ground pressure vary with the levels at which the key strata occur. During the mining of an extrathick coal seam with hard roofs, thick and hard strata with a ratio (of the distance from the coal seam to seam thickness) of 5.3–7.3 have the greatest influence on the working face

Data Availability

The data and material are transparent and included in the paper.

Conflicts of Interest

The authors declare that there is no conflict of interest.

Acknowledgments

We are grateful Yun Zhang, Lixin Lan, Baiyi Li, and Hao Yan for their assistance in physical simulation experiment. This work was supported by the State Key Research Development Program of China (grant numbers 2018YFC0604500, 2018YFC0604506), China Postdoctoral Science Foundation (grant number 2019M651080), applied basic research project of Shanxi Province (grant number 201901D211030), Scientific and Technological Innovation Programs of Higher Education Institutions in Shanxi (STIP) (grant number 2019L0208), Major Program in Shanxi Province (grant number 20191101015), and Independent Research Project of State Key Laboratory of Coal Resources and Safe Mining, CUMT (SKLCRSM18X006).

References

- [1] J. He, L. M. Dou, Z. L. Mu, A. Y. Cao, and S. Y. Gong, "Numerical simulation study on hard-thick roof inducing rock burst in coal mine," *Journal of Central South University*, vol. 23, no. 9, pp. 2314–2320, 2016.
- [2] G. F. Wang, S. Y. Gong, Z. L. Li, L. M. Dou, W. Cai, and Y. Mao, "Evolution of stress concentration and energy release before rock bursts: two case studies from Xingan coal mine Hegang China," *Rock Mechanics and Rock Engineering*, vol. 49, no. 8, pp. 3393–3401, 2016.
- [3] J. G. Ning, J. Wang, L. S. Jiang, N. Jiang, X. S. Liu, and J. Q. Jiang, "Fracture analysis of double-layer hard and thick roof and the controlling effect on strata behavior: a case study," *Engineering Failure Analysis*, vol. 81, pp. 117–134, 2017.
- [4] L. Bednarek and T. Majcherczyk, "An analysis of rock mass characteristics which influence the choice of support," *Geomechanics and Engineering*, vol. 21, no. 4, pp. 371–377, 2020.
- [5] T. Zhao, C. Y. Liu, K. Yetilmesoy, B. S. Zhang, and S. Zhang, "Fractural structure of thick hard roof stratum using long beam theory and numerical modeling," *Environment and Earth Science*, vol. 76, no. 21, p. 751, 2017.
- [6] X. L. Li, C. W. Liu, Y. Liu, and H. Xie, "The breaking span of thick and hard roof based on the thick plate theory and strain energy distribution characteristics of coal seam and its application," *Mathematical Problems in Engineering*, vol. 2017, 14 pages, 2017.
- [7] W. L. Shen, J. B. Bai, X. Y. Wang, and Y. Yu, "Response and control technology for entry loaded by mining abutment stress of a thick hard roof," *International Journal of Rock Mechanics and Mining Sciences*, vol. 90, pp. 26–34, 2016.
- [8] J. F. Ju and J. L. Xu, "Structural characteristics of key strata and strata behaviour of a fully mechanized longwall face with 7.0m height chocks," *International Journal of Rock Mechanics and Mining Sciences*, vol. 58, pp. 46–54, 2013.
- [9] B. W. Xia, J. L. Jia, B. Yu, X. Zhang, and X. L. Li, "Coupling effects of coal pillars of thick coal seams in large-space stopes and hard stratum on mine pressure," *International Journal of Mining Science and Technology*, vol. 27, no. 6, pp. 965–972, 2017.
- [10] B. Yu, J. Zhao, T. J. Kuang, and X. B. Meng, "In situ investigations into overburden failures of a super-thick coal seam for longwall top coal caving," *International Journal of Rock Mechanics and Mining Sciences*, vol. 78, pp. 155–162, 2015.
- [11] B. Yu, J. Zhao, and H. T. Xiao, "Case study on overburden fracturing during longwall top coal caving using microseismic monitoring," *Rock Mechanics and Rock Engineering*, vol. 50, no. 2, pp. 507–511, 2017.
- [12] H. W. Zhang, Z. J. Zhu, L. J. Huo, Y. Chen, and B. J. Huo, "Overburden failure height of superhigh seam by fully mechanized caving method," *Journal of China Coal Society*, vol. 39, no. 5, pp. 816–821, 2014.
- [13] B. Yu, R. Gao, X. B. Meng, and T. J. Kuang, "Near-far strata structure instability and associate strata behaviors in large space and corresponding control technology," *Chinese Journal of Rock Mechanics and Engineering*, vol. 37, no. 5, pp. 1134–1145, 2018.
- [14] J. X. Yang, C. Y. Liu, and B. Yu, "Mechanism of complex mine pressure manifestation on coal mining work faces and analysis on the instability condition of roof blocks," *Acta Geodynamica et Geomaterialia*, vol. 12, no. 1, pp. 101–108, 2015.
- [15] Y. W. Lan, R. Gao, B. Yu, and X. B. Meng, "In situ studies on the characteristics of strata structures and behaviors in mining of a thick coal seam with hard roofs," *Energies*, vol. 11, no. 9, p. 2470, 2018.
- [16] B. Yu, "Behaviors of overlying strata in extra-thick coal seams using top-coal caving method," *Journal of Rock Mechanics and Geotechnical Engineering*, vol. 8, no. 2, pp. 238–247, 2016.
- [17] H. M. Li, D. J. Jiang, and D. Y. Li, "Analysis of ground pressure and roof movement in fully-mechanized top coal caving with large mining height in ultra-thick seam," *Journal of China Coal Society*, vol. 39, no. 10, pp. 1956–1960, 2014.
- [18] R. Singh, P. K. Mandal, A. K. Singh, R. Kumar, J. Maiti, and A. K. Ghosh, "Upshot of strata movement during underground mining of a thick coal seam below hilly terrain," *International Journal of Rock Mechanics and Mining Sciences*, vol. 45, no. 1, pp. 29–46, 2008.
- [19] Z. Li, S. C. Yu, W. B. Zhu et al., "Dynamic loading induced by the instability of voussoir beam structure during mining below the slope," *International Journal of Rock Mechanics and Mining Sciences*, vol. 132, article 104343, 2020.
- [20] J. L. Xie and J. L. Xu, "Effect of key stratum on the mining abutment pressure of a coal seam," *Geosciences Journal*, vol. 21, no. 2, pp. 267–276, 2017.
- [21] B. Yu, Z. Zhang, T. J. Kuang, and J. R. Liu, "Stress changes and deformation monitoring of longwall coal pillars located in weak ground," *Rock Mechanics and Rock Engineering*, vol. 49, no. 8, pp. 3293–3305, 2016.
- [22] Y. Chen, S. Q. Ma, and Y. Yu, "Stability control of underground roadways subjected to stresses caused by extraction of a 10-m-thick coal seam: a case study," *Rock Mechanics and Rock Engineering*, vol. 50, no. 9, pp. 2511–2520, 2017.
- [23] W. B. Guo, H. S. Wang, G. W. Dong, L. Li, and Y. G. Huang, "A case study of effective support working resistance and roof support technology in thick seam fully-mechanized face mining with hard roof conditions," *Sustainability*, vol. 9, no. 6, p. 935, 2017.
- [24] D. Mondal, P. N. S. Roy, and M. Kumar, "Monitoring the strata behavior in the distressed zone of a shallow indian longwall panel with hard sandstone cover using mine-microseismicity and borehole televiewer data," *Engineering Geology*, vol. 271, article 105593, 2020.
- [25] D. Szurgacz and J. Brodny, "Analysis of the influence of dynamic load on the work parameters of a powered roof

- support's hydraulic leg," *Sustainability*, vol. 11, no. 9, article 2570, 2019.
- [26] P. Konicek and P. Waclawik, "Stress changes and seismicity monitoring of hard coal longwall mining in high rockburst risk areas," *Tunnelling and Underground Space Technology*, vol. 81, pp. 237–251, 2018.
- [27] M. G. Qian, X. X. Miao, and J. L. Xu, "Theoretical study of key stratum in ground control," *Journal of China Coal Society*, vol. 21, no. 3, pp. 225–230, 1996.
- [28] X. X. Miao and M. G. Qian, "Advance in the key strata theory of mining rockmass," *Journal of China University of Mining and Technology*, vol. 1, pp. 25–29, 2000.
- [29] H. Yan, J. X. Zhang, S. Zhang, and N. Zhou, "Physical modeling of the controlled shaft deformation law during the solid backfill mining of ultra-close coal seams," *Bulletin of Engineering Geology and the Environment*, vol. 78, pp. 3741–3754, 2019.
- [30] J. F. Ju and J. L. Xu, "Surface stepped subsidence related to top-coal caving longwall mining of extremely thick coal seam under shallow cover," *International Journal of Rock Mechanics and Mining Sciences*, vol. 78, pp. 27–35, 2015.
- [31] R. Gao, B. J. Huo, H. C. Xia, and X. B. Meng, "Numerical simulation on fracturing behaviour of hard roofs at different levels during extra-thick coal seam mining," *Royal Society Open Science*, vol. 7, no. 1, article 191383, 2020.